JOURNAL OF MATERIALS SCIENCE 28 (1993) 3581–3588

Semi-solid deformation in multi-component nickel aluminide

Part I *Equiaxed alloys*

C. S. LIN, J. A. SEKHAR
Department of Materials Science and Engineering, University of Cincinnati, Cincinnati, OH 45221-0012, USA

A systematic study was carried out to determine the solidification and tensile behaviour of semi-solid multi-component nickel aluminide. Controlled equiaxed-solidified samples were tested at various temperatures in the mushy (semi-solid) region. A special Gleeble testing procedure was developed where the samples were quickly raised to a predetermined temperature in the semi-solid zone and fractured. The fracture stress was noted to decrease monotonically with temperature. The strain to fracture exhibited a ductility minimum at an intermediate temperature in the semi-solid zone. For the equiaxed-solidified samples, the fracture stress was found to decrease with increasing cooling rate at any given temperature. At the temperature corresponding to the strain minimum, residual microcracks were detected on the fracture surface. The upper hot-tearing temperature was found to be a function of the solidification variables. The amount of strain accommodation and the hot tearing resistance was found to be a function of solidification microstructure. A fracture map, which is the fracture stress, temperature and cooling rate (σ_f–T–$\dot{T}$) diagram for the equiaxed microstructures, is presented and a castability map is created from the fracture data.

1. Introduction

The majority of defects in a casting are established during the solidification stage where both liquid and solid coexist (i.e. the mushy zone). A knowledge of the properties of the semi-solid mass are thus important for determining the proper processing parameters during casting. In this paper, we examine the influence of the solidification morphology on the mechanical properties of the mushy zone in the multi-component nickel aluminide alloy IC396M (Table I). The processing map for obtaining tear-free castings with equiaxed solidification structure is also discussed. A typical castability map for obtaining tear-free castings is developed for the IC396M alloy.

Nickel aluminide intermetallic compositions (Ni_3Al type) containing boron are being considered for use as new structural materials because of their outstanding properties related to cavitation, erosion, high-temperature oxidation, wear, and fatigue resistance as well as their low density [1]. Optimizing properties in these alloys has led to the binary composition of nickel aluminide being assayed with several elements, e.g. zirconium, chromium, iron, molybdenum, cerium and boron. Zr is a solid-solution strengthener and increases high-temperature strength and ductility. Cr alleviates the lack of ductility at intermediate temperatures. Mo is a solid-solution strengthener especially helpful at high temperatures, and B ductilizes the alloy by disordering the grain boundaries. Oxygen is detrimental as it is known to give rise to dynamic embrittlement and medium-temperature loss of ductility. The solidification sequence of the alloy has been discussed earlier [2], following the modified Ni–Al phase diagram [3,4] which indicates that primary γ' (Ni_3Al) forms during cooling, prior to the eutectic formation. In the earlier study [2], it was shown conclusively that microporosity was associated with the primary γ' and that this microporosity was related to the imposed processing conditions through the dendrite formation parameters. The microporosity formed well behind the dendrite tip and was considered to be an intrinsic feature of the solidification structure.

Hot tearing takes place between the temperature at which the solid becomes coherent and the end of freezing, i.e. the solidus [5–9]. Hot tearing occurs if the mould-imposed tensile stress in the semi-solid region exceeds the fracture stress. If further healing of this fracture by the adjacent liquid is not possible, then the cracks remain in a cast sample. Even if further healing is possible, the healed region may show gross segregation [10–12]. Thus, it is important to obtain information on the magnitude of the cracking stresses in the semi-solid region below the coherency temperature (i.e. the temperature below which the semi-solid strength will develop). The fracture strains in the semi-solid region are expected to be smaller than those for the temperature region just below the solidus.

Hot tearing is influenced by several variables. The grain size of a cast metal has been recognized to influence the semi-solid properties in both shear and

0022–2461

TABLE I Composition of alloy IC396M

Element	Composition (wt %)
Ni	80.42
Al	7.98
Cr	7.72
Mo	3.02
Zr	0.85
B	0.005–0.01

tensile testing [5–9]. The imposed strain rate in compression has been shown to influence macrosegregation as well as influence the semi-solid strength [10]. There have been investigations into the role of gas content [13], composition [14, 15] and porosity [16] on the hot tearing tendency. In general, it seems that the most important variables are those of contraction hindrance, temperature gradient and grain size [8, 15, 17, 18]. It has been found that a reduction in grain size leads to a reduction of hot tearing. In terms of the thin-film theory [18], a fine grain size implies an abundant network of liquid films. This network, because of higher strain accommodation in the liquid, is more easily deformed for a smaller grain size than a higher grain size. Kubota and Kitaoka [6] conclude that a reduction in grain size (achieved for example by adding grain refiners) leads to a lowering of the coherency temperature. They further show that this changes the fracture stress–temperature relationship. Additionally, as the amount of linear contraction also decreases, a small grain size leads to a lowering of the hot tearing tendency. The implication of the work reported by Kubota and Kitaoka [6] is that the strain during solidification is lower if the coherency range is small. The indirect measure of this strain is the slope of the fracture stress–temperature curve. (There is, however, some concern about whether the experimental data shown by Kubota and Kitaoka justify the linear relationship described by them.) Kubota and Kitaoka also show an example where a transition from columnar to equiaxed microstructure reduces the hot tearing tendency. Similar ideas have previously been discussed by Borland [5] and Flemings [19] (i.e. of relating the coherency range directly with the hot tearing tendency of dendritic alloys). Reducing the coherency range by continuous shearing during solidification or reducing the shear strength of dendrites in the presence of thin liquid films may also be used as a means for casting tear-free alloys in their semi-solid state [10, 11, 20–26].

At lower temperatures, especially when small amounts of insoluble (in the solid) solute are present, a microcracking phenomena may manifest itself [5, 15–18]. The microcracks are most likely to form when almost continuous films of liquid are present in a predominantly solid structure. The spread of this liquid is a function of the magnitude of the liquid–solid energy relative to that of the grain boundary energy [5]. If this ratio is close to 0.5, then the liquid film is evenly spread, leading to easy microcracking. If the ratio is higher, then cracking is more difficult as the film may no longer be continuous. The issue of crack initiation for this microcracking phenomenon has not been studied. The influence of these residual microcracks on the hot tearing tendency when a casting is reheated has also not been addressed in the literature.

Similar liquid film microcracking is noted during welding operations. Nickel-base superalloys (similar in composition to the IC396M alloy and containing Nb) are prone to hot cracking in the weld heat-affected zone (HAZ). This hot cracking has been attributed to the constitutional liquation of niobium carbide (NbC) in wrought alloys [27] and both NbC and Laves phase [28–32] in cast alloys. Hot microcracking is produced by the presence of a liquid film along grain boundaries [33] and the inability of this film to resist the stresses produced as the weld HAZ cools down. The existence of a grain boundary liquid is not sufficient for hot cracking to occur. The liquid film produced on heating must exist until stresses begin to be developed in the HAZ, and the liquid must remain wetted on the grain boundaries over this temperature range. As the intergranular liquid forms during rapid heating, its chemistry is modified by the local chemistry in the grain boundary region. Heat treatments [34] can alter the free surface chemistry of certain elements and may also be expected to alter the intergranular chemistry in the liquid. As the HAZ cools down, the distribution of this chemistry-modified liquid along the grain boundaries depends on the freezing point, the liquid–solid interfacial energy, and the variation of this energy with temperature. These factors strongly influence the hot cracking susceptibility of the alloy.

It has been shown in several investigations [31, 34] that solution-annealing reduces microfissuring susceptibility, while age-hardening increases it. Thompson and Genculu [27] observed the beneficial effect of solution-annealing and the detrimental effect of age-hardening on microfissuring. They studied wrought alloys and found that microfissuring was initiated by the constitutional liquation of niobium-rich M(C, N) particles. Intergranular liquid produced by this reaction was found in both the solution-annealed and age-hardened condition. They suggested that the microfissuring differences due to these heat treatments were related to the manner in which the intergranular liquid distribution was controlled by intergranular chemistry. It was postulated that heat treatment alters the intergranular chemistry in such a way that microfissuring susceptibility may either be increased or reduced [34]. It is now known that increasing the grain size, independent of other variables, causes an increase in the microfissuring susceptibility [31]. Thus, microfissuring has some functional dependence on a grain size variable, such as the grain boundary surface area. The apparent relation with grain size would indicate that the cracking problem associated with the weld HAZ is of an intergranular nature, and is caused by either low-melting or brittle grain boundary films. If such films were present, a coarse grain size would effectively reduce the total grain boundary area of the weld HAZ, thus concentrating the films and increasing their deleterious effects. It will be noted

below that similar film formation issues are important for castings.

For the case where dendrites are present, Ackermann *et al.* [26] have indicated that if the dendrites are separated by a continuous liquid film, the resistance to tensile stresses is very low and due mainly to friction and bending forces between dendrite arms. From other observations they concluded that, at a solid fraction of about 0.95, the interdendritic liquid may change from a continuous film to discontinuous droplets enclosed in the solid [26]. It is supposed that, for solid fractions less than 0.95, the mechanical strength of the section is low and that above this value the material possesses its full strength. A strain rate exponent of ~ 0.34 was calculated by Ackermann *et al.* [26] for the deformation of Al–Mg alloys close to the solidus temperature and in which the orientation of the solidifying microstructure could be controlled with respect to the testing.

The upper temperature in the coherent range is an ambiguous parameter, not properly defined in the literature. The amount of solid formed prior to the onset of coherency has been assumed to be as low as 60% [6] and as high as 95% [26]. Alloy composition variables leading to morphological changes in the solidification morphology seem to influence this number, although this aspect has never been systematically studied. Prevalent also is some overlap regarding the definition of the onset of coherency and the onset of residual hot tearing [5, 7, 9, 15, 35, 36]. Results described in the literature seem to indicate that in long-freezing-range alloys, coherency may develop well ahead (i.e. at a lower fraction of solid) of the residual hot tearing. Although fracture of the material is possible soon after coherency, the only residual effect of this at a low fraction of solid is likely to manifest itself in an observed change of morphology where stress (or shear) influences solidification microstructure evolution and macrosegregation. Additionally, as mentioned above, filled tears may show gross macrosegregation [10–12]. At a higher fraction of solid, the microstructure has established a well-defined spacing and the stresses may cause cracking which remains in the casting. There has been little or no attempt at studying the fracture phenomenon *vis-à-vis* the established solidification microstructure. This is the aim of this paper.

In this paper, carefully grown controlled equiaxed microstructures were tested for strength and ductility at various temperatures in the semi-solid range. The samples were obtained from studies reported previously [2, 37]. These previous studies [2, 37] were aimed at understanding the residual solidification microporosity. For this, all the relevant dendrite scales were carefully recorded and correlated with residual microporosity [2, 37]. Thus, the samples were well characterized prior to testing in the semi-solid state. In addition, the samples possessed microporosity associated with the primary γ' which presumably prevented any problems associated with the initiation of microcracking. In this paper the onset of microcracking is also discussed from an observation of the strain to fracture. Residual microcracking in solidified structures is also critically examined.

2. Experimental procedure

The strength in the semi-solid zone was measured with a Gleeble unit (a thermomechanical testing device manufactured by Duffers Scientific , Inc.). The Gleeble machine had three main systems which included the hydraulic servo-mechanical system, the computer control system and the data acquisition system. A Macintosh SE computer, 16-bit data acquisition card (ACSE-16-8), terminal panel (T51) and Analog Connection Workbench software was utilized for the data acquisition system. This system contained eight differential analogue inputs, eight digital I/O lines,

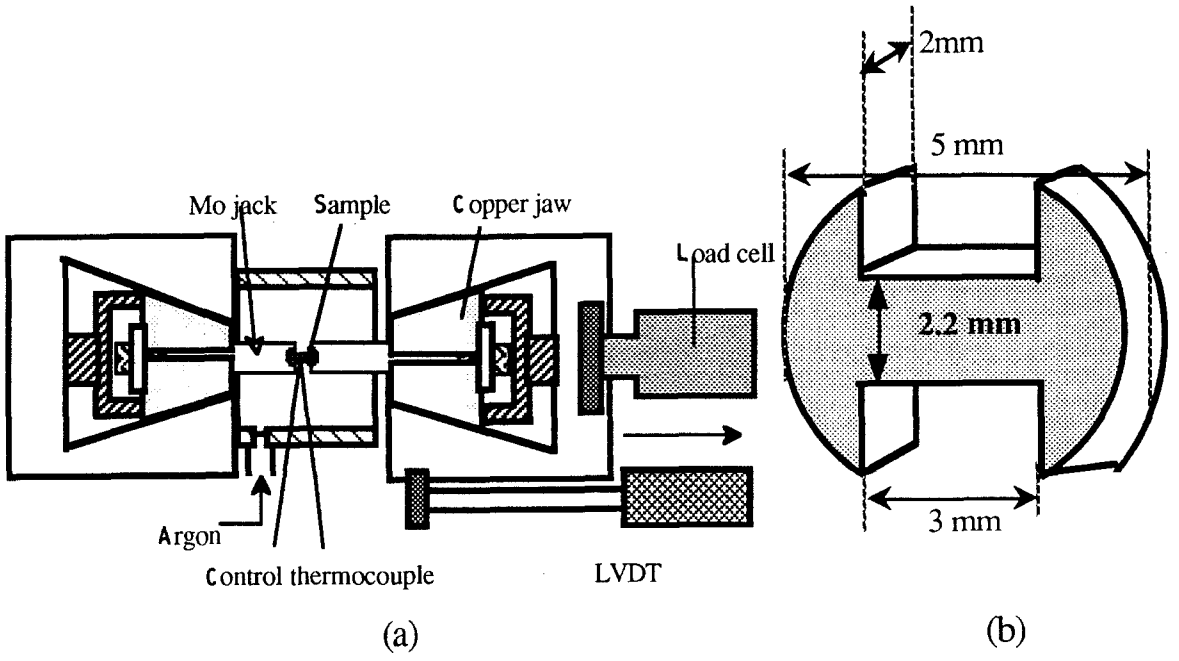

Figure 1 (a) Schematic diagram of the Gleeble and (b) sample dimensions.

acquisition speeds from 2.5 to 225 kHz, and a high-noise-rejection converter. Five channels were used in the system. Data points were acquired approximately 20–30 ms apart.

Samples of IC396M which were cast under conditions of different cooling rates were utilized. The test samples were shaped as shown in Fig. 1. Some samples were grain-refined by the addition of cobalt aluminate [38]. Two molybdenum bars were shaped as jacks for the Gleeble test (Fig. 1). K-type thermocouples of diameter 0.24 mm were used for the control sensor and argon was introduced in the testing container to avoid oxidation. The thermocouples were attached directly to the sample. The Gleeble Programming Language (GPL) software was used to control the heating rate. The heating of the samples was carried out up to the semi-solid temperature at a constant rate and the samples were then tested to failure. The time to heat the specimen to the desired temperature was approximately 60 s. Failure of the sample after deformation resulted in the opening of the circuit, which in turn prevented further passage of current and allowed the sample to cool quickly to room temperature. The jaws were programmed to move at a speed of 0.2 mm s^{-1} when no sample was held between the jaws.

It has been previously shown [39–41] that the nature of fracture and the fracture strain may be different when measured at the same temperature for solidification and for reheating. Reheated alloys tend to display somewhat higher values of fracture stress [39, 40]. In this paper all measurements reported are from reheated specimens only. The limitation of such measurements has also been discussed below. The rate of heating to the desired temperature was approximately 20 K s^{-1}. The fracture surface always intersected the point at which the thermocouple was placed (i.e. the midpoint of the gauge). We estimate our results to have a $\pm$ 5 K accuracy as the temperature gradient measured in the mid-section of the sample was of the order of 10 K mm^{-1}.

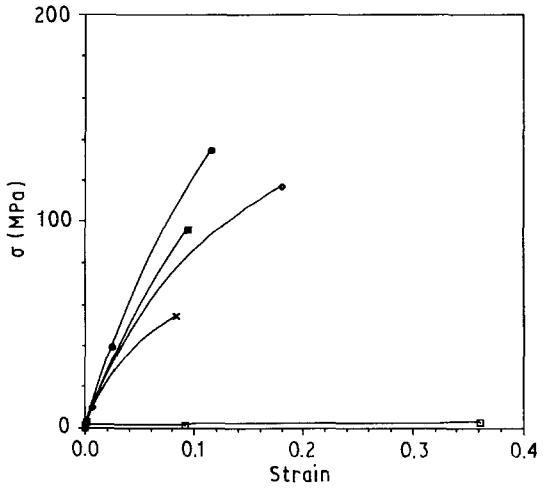

Figure 2 Stress–strain relationship for equiaxed-solidified microstructure at a cooling rate of 0.05 K s^{-1} and temperature (●) 1328 K, (◆) 1367 K, (■) 1391 K, (×) 1408 K, (⊡) 1496 K.

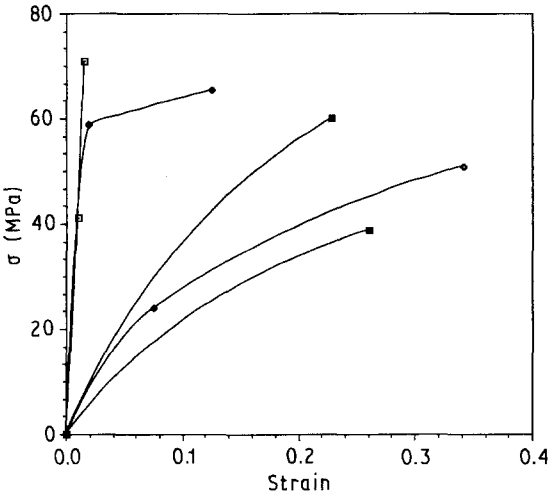

Figure 3 Stress–strain relationship of original IC396M (swaged) alloy at (⊡) 1342 K, (◆) 1389 K, (■) 1420 K, (◆) 1476 K, (■) 1498 K.

3. Results and discussion

3.1. Stress–strain relationship in the semi-solid zone

Stress–strain relationships were obtained with the Gleeble at temperatures ranging from 1300 to 1543 K for the equiaxed-solidified microstructures. The lowest temperature was lower than the lowest melting eutectic in the alloy [2] and the highest temperature was the temperature at which the alloy developed no strength. A typical relationship is shown in Fig. 2. The stress–strain relationships of the original IC396M (swaged) alloy are also shown in Fig. 3.

In this paper strength is measured and plotted as a function of temperature and not fraction of liquid because (a) the fraction of liquid is a function of the solidification conditions and not simply of the temperature, and (b) the fraction of liquid at 1543 K (the upper measurement temperature) is low and we have found it difficult to obtain accurate data on the fraction of liquid from the quench microstructure at these high solid fractions. This is especially true at the lower temperatures in the semi-solid region. Additionally, the fracture maps given below are more useful to employ in this study, with the temperature forming one of the axes, than when the fraction of solid is used as a variable. The estimated liquidus temperature for IC396M is 1655 K [2].

3.2. Fracture in the equiaxed-solidified alloy and ductility minima

Mechanical properties were obtained from equiaxed samples solidified at four carefully controlled cooling rates with and without grain refiner [37]. The cooling rates employed are shown in Table II [38]. As the cooling rate increased the stress to failure was found to decrease at a given temperature, as shown in Fig. 4. Similarly the upper hot tearing temperature increases with decreasing cooling rate provided comparison is made for an equivalent amount of grain refiner. At the higher cooling rates, finer secondary arm spacings and

TABLE II Cooling rates and grain sizes of equiaxed solidified samples [38]

Cooling rate	Grain size (μm)	
($K s^{-1}$)	Without grain refiner	With grain refiner
0.05	27500	4330
0.50	5020	–
3.31	1500	580
12.5	380	260

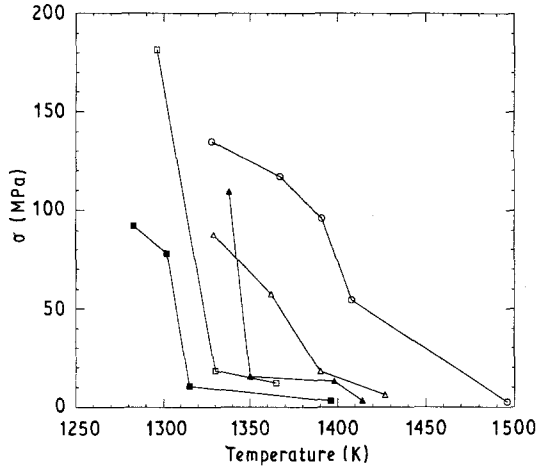

Figure 4 Stress to failure versus temperature for equiaxed-solidified IC396M at various imposed cooling rates: (○) 0.05 $K s^{-1}$, (△) 0.50 $K s^{-1}$, (▲) 3.31 $K s^{-1}$, (□) 12.5 $K s^{-1}$, (■) 12.5 $K s^{-1}$ (grain-refined).

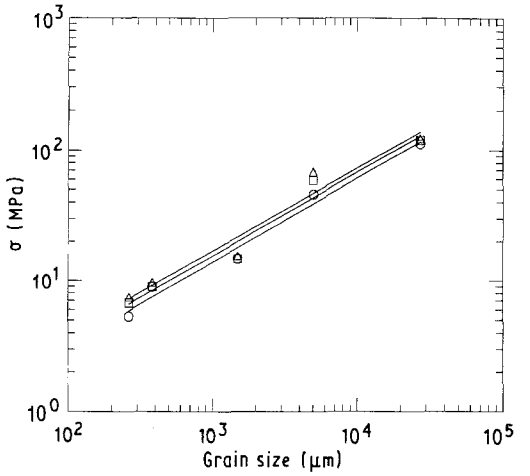

Figure 5 Fracture stress at a given temperature as a function of the grain size for equiaxed-solidified IC396M at (△) 1350 K, (□) 1360 K, (○) 1370 K.

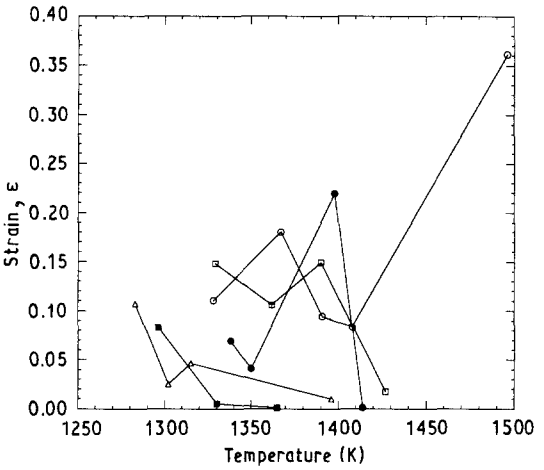

Figure 6 Strain at failure ε versus temperature for equiaxed-solidified IC396M. Cooling rate (○) 0.05 $K s^{-1}$, (□) 0.50 $K s^{-1}$, (●) 3.31 $K s^{-1}$, (■) 12.5 $K s^{-1}$, (△) 12.5 $K s^{-1}$ (grain-refined).

smaller grains were noted [37, 38]. As a result, a larger grain boundary area was obtained. Since grain boundaries were weak at high temperature, especially in the presence of a liquid film, lower fracture stresses were noted at the higher cooling rates. The effect of grain size on the fracture stress at a given temperature is shown in Fig. 5.

Some minima in the plot of fracture strain as a function of temperature were noted for the equiaxed morphologies (Fig. 6). A film-like residue was noted on the fracture surface at this temperature. This is discussed further in Part II [42]. A minimum in the fracture strain with temperature for equiaxed Pb–Sn alloys has previously been documented at low strain rates [41]. With an increase in the strain rate, the minimum was no longer noted [41]. Fig. 7 shows the plot of the temperature $T(\varepsilon_{\min f})$ for equiaxed casting as a function of the cooling rate for the samples which were not grain refined. If an intermediate temperature ductility minimum was not observed, then the lowest ductility temperature was taken for Fig. 7. A transition of the temperature of the strain minimum $T(\varepsilon_{\min f})$, from 1420 to 1360 K at around a 0.1 $K s^{-1}$ cooling rate was noted. It will be noted in Part II [42] that the two ductility minimum temperatures for the equiaxed structures fall along the ductility minimum bands for the directionally solidified structures. In particular, the lower ductility minimum corresponds to the transverse directionally solidified minimum and the higher ductility minimum corresponds to the longitudinal directionally solidified minimum.

3.3. Hot tearing susceptibility

The hot tearing resistance is related to the amount of strain accommodation that is possible [8, 15, 17, 18, 20–26, 43, 44], although alternative definitions are available when lower fractions of solid are considered [45, 46]. Lower grain sizes in equiaxed castings are known to be more resistant to hot tearing than the higher grain sizes [5–9].

An examination of Fig. 4 indicates that the upper coherency temperature decreases with an increase in the cooling rate, thus explaining the noted effect of grain size on hot tearing. Additionally, a lack of the intermediate temperature ductility minimum with an increase in the cooling rate may have an impact on the hot tearing resistance.

A comparison of hot tearing in equiaxed and directionally solidified samples is given in Part II [42]. The influence of dendrite-to-equiaxed transition on the hot tearing tendency is also discussed in Part II.

3.4. Fracture maps for nickel aluminide

Fracture maps may be defined as the processing–property maps which may critically affect casting design. These maps should reflect conditions for which casting will tear. The fracture map for IC396M has been developed after a critical examination of the solidified microstructure and the semi-solid strengths. The fracture map is the σ_f–T–$\dot{T}$ (i.e. fracture stress–temperature–cooling rate) plot for equiaxed microstructure. This is shown in Fig. 8. The temperature $T(\varepsilon_{\min f})$ for the equiaxed samples is also shown in the fracture map, as this is the temperature at which residual microcracks may be left in a casting.

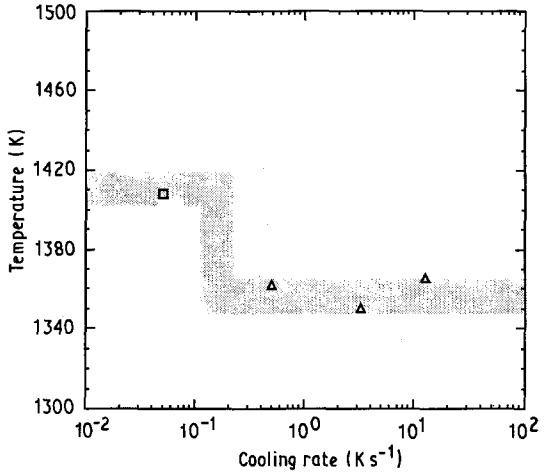

Figure 7 Plot of the temperature of minimum ductility $T(\varepsilon_{\min f})$ as a function of the cooling rate for samples which were not grain-refined. □ and △ represent the upper and lower film formation temperatures respectively.

3.5. Castability maps for equiaxed castings

The important processing variable in equiaxed casting is the cooling rate $\dot{T}$. Fig. 9 shows the plot of the ratio of imposed stress to the fracture stress at a given temperature as a function of cooling rate. Table III shows the measured mechanical properties of the alloy IC396M. This data were used to draw Fig. 9. The thermal expansion coefficient α is taken to be 13.6 $\times 10^{-6}$ K^{-1} for the alloy, σ_f is the fracture stress at a given temperature T, and E_T is the measured modulus at the same temperature. The quantities σ_f and E_T are measured from plots such as Fig. 2. Below 1360 K there is very little liquid. However, because the amount of measured primary γ' particles varies with cooling rate (Fig. 10), the measured modulus below 1360 K will be different for the four cooling rates. The higher the primary γ', the lower the effective measured modulus. This modulus affects the curve at 1329 K shown in Fig. 9, where a peak in the curve is noted for a cooling rate of 0.5 K s^{-1}. For a casting which has already developed microcracks at the ductility minimum temperature, the stress for the 0.5 K s^{-1} cooling rate may be high enough to cause propagation of the crack.

4. Conclusions

This paper is the first report of systematic measurement of semi-solid stress–strain relationships for equiaxed solidified alloys. Part II [42] similarly contains information on directional dendrites. The following are the main conclusions of the work:

1. Gleeble testing has been shown to be a unique way of determining the mechanical behaviour of semi-solid materials. The testing was employed successfully

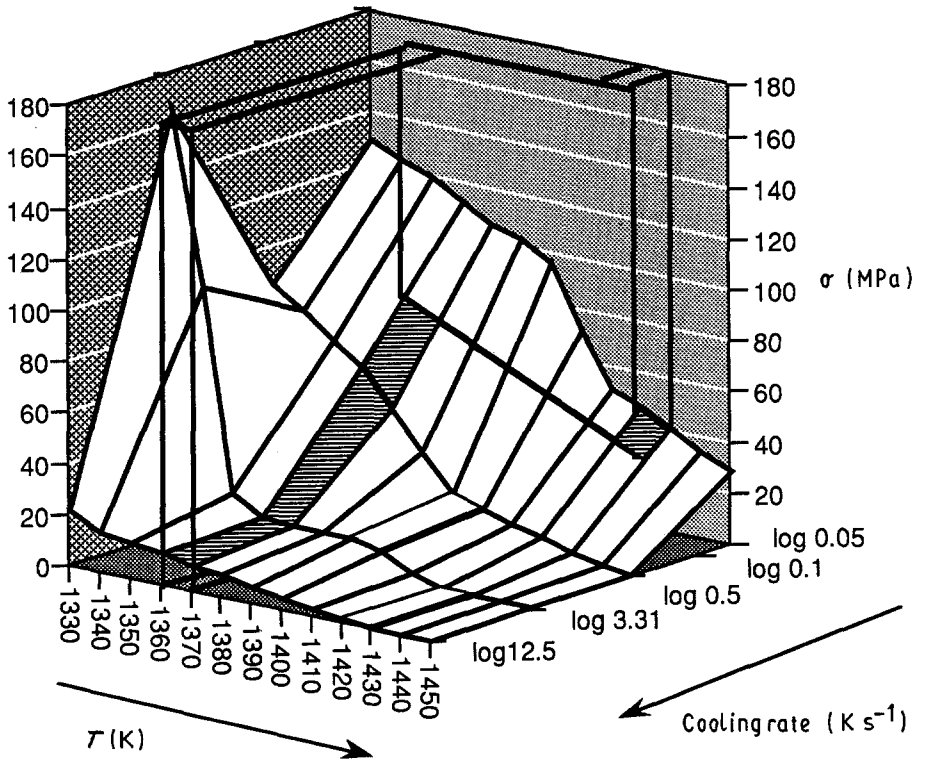

Figure 8 Three-dimensional fracture map (stress–temperature–cooling rate) for equiaxed-solidified IC396M. The shaded region is the temperature at which the minimum in the fracture strain was observed.

TABLE III Measured mushy zone properties from stress-free equiaxed solidified samples

Cooling rate ($K s^{-1}$)	T(K)	E_T(MPa)	σ_f(MPa)	$\frac{\alpha E_T(T_L - T)}{\sigma_f}$
3.31	1453	274	3.617	0.2005
	1398	180	13.06	0.0482
	1350	380	15.52	0.1016
	1338	1589	109.6	0.0625
0.5	1427	380	6.192	0.1903
	1390	117	18.02	0.0234
	1362	545	57.52	0.0378
	1329	2200	89.91	0.2648
0.05	1496	3.68	2.633	0.0030
	1408	651	54.50	0.0401
	1391	1717	95.99	0.0642
	1367	1200	116.9	0.0402
	1328	1505	134.7	0.0523
12.5	1365	830.8	12.15	0.2696
	1330	1419	18.46	0.2673
	1296	2046	181.5	0.0550
12.5 (grain-refined)	1396	142.5	3.170	0.1583
	1315	248.1	10.66	0.1076
	1302	3134	78.22	0.1923
	1283	879.5	92.31	0.0482

α is taken to be $13.6 \times 10^{-6}\ K^{-1}$ for the alloy. E_T is the measured modulus at a given temperature T. T_L the liquidus temperature. σ_f is the fracture stress at the same temperature. The modulus E_T is determined from the average slope between the first two or three data points of the type shown in Fig. 2. This modulus may somewhat underestimate the slope at the origin.

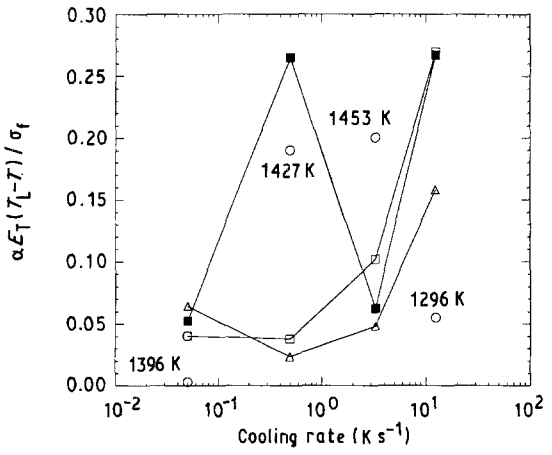

Figure 9 Ratio of imposed stress to fracture stress at a given temperature versus cooling rate for IC396M at various temperatures: (■) 1329 K, (□) 1360 K, (△) 1391 K. α is taken to be $13.6 \times 10^{-6}\ K^{-1}$ for the alloy. E_T is the measured modulus at a given temperature T. T_L is the liquidus temperature. σ_f is the fracture stress at the same temperature. This is the equiaxed solidified castability map for this alloy. Note that if a casting is stressed at and below 1360 K then residual micro-cracks may remain in the casting.

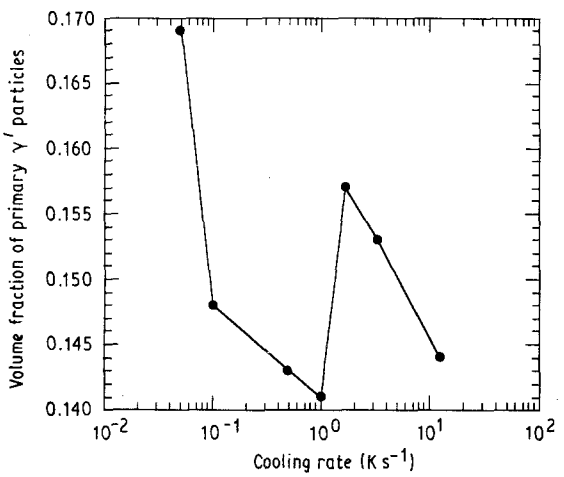

Figure 10 Volume fraction of primary γ' particles in IC396M alloy. Note that a minimum occurs at a cooling rate of 0.5 $K s^{-1}$.

for the study of the semi-solid mechanical properties of multicomponent nickel aluminide.

2. There exists a critical temperature (for equiaxed samples) in the semi-solid region at which there is a strain minimum. This temperature is $\sim$ 1360 K for cooling rates $> 0.1\ K s^{-1}$ in equiaxed tested samples. The microstructural implications of the strain minimum are being examined; however, preliminary examination of fractographs indicates that the temperature is related to the formation of a thin liquid film. The lower temperature of 1360 K is also the temperature at which residual microcracks may be left behind in the solidified structure.

3. Increasing $\dot{T}$ in equiaxed samples leads to an increase in the fracture strain and thus an increase in the hot cracking resistance. Fracture maps (processing maps) may be generated. The information from the fracture map σ_f–T–$\dot{T}$ along with the modulus data may be recast into castability maps to be used for the design of castings.

4. The solidification and cooling rates selected for this study lie in the range of cooling rates commonly employed commercially for casting purposes. For a casting process we may obtain information on $\dot{T}$ during solidification. In addition it is fairly simple to estimate the magnitude of mould-imposed stress on a

casting [19, 41, 47–49]. By comparing the values with the σ_f–T–$\dot{T}$ plot, it may be determined whether there is any value that lies above the net. If a problem is anticipated, parameters like mould design, cooling rate etc. may be changed to ascertain that there is no processing condition above the critical values shown on the net. In addition, stresses at $T(\varepsilon_{\min f})$ should be kept as low as possible to avoid residual microcracks. If microcracks do form, then their propagation depends on the microstructure (γ' content) which an imposed cooling rate has generated.

Acknowledgements

This work was performed as a part of Edison Material Technology project CT-17 monitored by Dr E. F. Moore and Dr L. Midolo. Dr Harold Gegel was task leader of the project. The alloys were obtained from Oak Ridge National Laboratory and Armco steel for which we express our gratitude to Dr V. Sikka and Dr R. O'Malley. The authors thank Professor K. Challenger for allowing us the use of the Gleeble Unit and for valuable discussions. Discussions with Dr A. Gokhale are also gratefully acknowledged.

References

1. V. K. SIKKA, *Mater. Manuf. Processes* **4** (1989) 1.
2. C. T. HO, C. J. CHENG and J. A. SEKHAR, *Metall. Trans. A* **22A** (1991) 225.
3. J. D. VERHOEVEN, J. H. LEE, F. C. LAABS and L. L. JONES, *J. Phase Equil.* in press.
4. F. J. BREMER, M. BEYSS, E. KARTHAUS, A. HELLWIG, T. SCHOBER, J. M. WELTER and H. WENZEL, *J. Cryst. Growth* **87** (1988) 185.
5. J. C. BORLAND *Br. Weld. J.* **7** (1969) 508.
6. M. KUBOTA and S. KITAOKA, *AFS Trans.* **81** (1973) 424.
7. S. W. METZ and M. C. FLEMINGS, *ibid.* **78** (1970) 453.
8. *Idem, ibid.* **77** (1969) 329.
9. J. C. BORLAND, *Weld. Met. Fabricn* (March 1979) 99.
10. M. SUERY and M. C. FLEMINGS, *Metall. Trans. A* **13A** (1982) 1809.
11. C. Y. CHEN, J. A. SEKHAR, D. BACKMAN and R. MEHRABIAN, *J. Mater. Sci. Eng.* **40** (1980) 265.
12. M. C. FLEMINGS and R. MEHRABIAN, *AFS Trans.* **81** (1973) 81.
13. R. A. FLINN, "*Fundamentals of Metal Casting*" (Addison-Wesley, 1963)
14. D. C. G. LEES, *J. Inst. Metals* **72** (1946) 343.
15. H. F. BISHOP, C. G. ACKERLAND and W. S. PELLINI, *AFS Trans.* **65** (1957) 247.
16. M. D. BRYANT, *Foundry* **95** (February, 1967) 78.
17. A. COUTURE and J. O. EDWARDS, *AFS Trans.* **81** (1973) 453.
18. W. S. PELLINI, *Foundry* (November, 1952) 125.
19. M. C. FLEMINGS, "*Solidification Processing*" (McGraw-Hill, New York, 1974).
20. D. A. PINSKY, P. O. CHARREYRON and M. C. FLEMINGS, *Metall. Trans. B* **15B** (1984) 173.
21. P. O. CHARREYRON and M. C. FLEMINGS, *Int. J. Mech. Sci.* **27** (1985) 781.
22. A. L. LUX and M. C. FLEMINGS, *Metall. Trans. B* **10B** (1979) 71.
23. D. G. BACKMAN, R. MEHRABIAN and M. C. FLEMINGS, *ibid.* **8B** (1977) 471.
24. F. E. GOODWIN, P. DAVAMI and M. C. FLEMINGS, *Metall. Trans. A* **11A** (1980) 1771.
25. T. MATSUMIYA and M. C. FLEMINGS, *Metall. Trans. B* **12B** (1981) 17.
26. P. ACKERMANN, W. KURZ and W. HEINEMANN, *J. Mater. Sci. Eng.* **75** (1985) 79.
27. R. G. THOMPSON and S. GENCULU, *Welding J.* **62** (1983) 337s.
28. W. A. BAESLACK III and D. E. NELSON, *Metallography* **19** (1986) 371.
29. B. RADHAKRISHNAN and R. G. THOMPSON, *Metall. Trans. A* **20A** (1989) 2866.
30. *Idem., Metallography* **21** (1988) 453.
31. R. G. THOMPSON, D. E. MAYO and B. RADHAKRISHNAN, *Metall. Trans. A* **22A** (1991) 557.
32. R. G. THOMPSON, J. J. CASSISMUS, D. E. MAYO and J. R. DOBBS, *Welding J.* **64** (1985) 91s.
33. J. C. BORLAND and R. N. YOUNGER, *Br. Weld. J.* **7** (1960) 22.
34. R. G. THOMPSON, J. R. DOBBS and D. E. MAYO, *Welding J.* **65** (1986) 299s.
35. A. R. E. SINGER and S. A. COTTRELL, *J. Inst. Metals* **73** (1947) 33.
36. R. A. ROSENBURG, M. C. FLEMINGS and H. F. TAYLOR, *AFS Trans.* **68** (1960) 518.
37. C. J. CHENG and J. A. SEKHAR, in proceedings of Conference on High Temperature Ordered Alloys, edited by L. A. Johnson, D. P. Pope and J. O. Stiegler, Materials Research Society Conference Proceedings Vol. **213** (1991) p. 853.
38. *Idem.*, "Solidification Microporosity in IC396M: Nickel Aluminide", (Vol. 2 of Final Report, "Equiaxed solidification" (Oak Ridge National Laboratory, 1990)
39. H. G. SUZUKI, S. NISHIMURA and S. YAMAGUCHI, *Trans. ISI Jpn* **22** (1982) 48.
40. K. KINOSHITA, G. KASAI and T. EMI, in "Solidification and Casting of Metal" (Metals Society, London, 1979) p. 268.
41. A. A. GOKHLE, *Trans. Indian Inst. Metals* **39** (1986) 153.
42. C. S. LIN and J. A. SEKHAR, *J. Mater. Sci.* **28** (1993) 3885.
43. C. M. SELLAR, *Int. Met. Rev.* **17** (1972) 1.
44. J. K. BRIMACOMBE, F. WEINBERG and E. B. HAWBOLT, *Metall. Trans. B* **10B** (1979) 279.
45. T. W. CLYNE and G. J. DAVIES, in "Solidification and Casting of Metal" (Metals Society, London, 1979) p. 275.
46. L. KATGERMAN, *Light Metals* (1980) 845.
47. A. ETIENNE and A. PALMERS, in "Solidification and Casting of Metal", (Metals Society, London, 1979) p. 295.
48. A. GRILL, J. K. BRIMACOMBE and F. WEINBERG, *JISI* **211** (1976) 34.
49. J. MATHEW and H. D. BRODY, in "Solidification and Casting of Metal" (Metals Society, London, 1979) p. 244.

Received 2 June
and accepted 17 November 1992